

Numerical investigation of recombination gain in the Li III transition to ground state

Y. Avitzour and S. Suckewer

Princeton University, Princeton, New Jersey 08540, USA

E. Valeo

Princeton Plasma Physics Laboratory, Princeton, New Jersey 08540, USA

(Received 17 October 2003; revised manuscript received 26 January 2004; published 30 April 2004)

We present a numerical investigation of the parameters characterizing the $2 \rightarrow 1$ transition recombination gain in Li III ions (13.5 nm). The numerical model includes the initial optical field ionization of the plasma by an intense 100 fs laser pulse, taking into account above threshold ionization heating, particle collisions, and spatial effects. Gain is then calculated during the process of recombination as the plasma expands and cools. We show that by taking into account the non-Maxwellian nature of the electron distribution function in the plasma and its spatial distribution, high gain in the $2 \rightarrow 1$ transition of Li III is feasible under certain initial conditions, even though initial estimates based on the energy absorption during the ionization predict very low gain. We characterize the behavior of the gain under different pumping parameters and initial plasma conditions.

DOI: 10.1103/PhysRevE.69.046409

PACS number(s): 52.25.Jm, 42.55.Vc, 32.80.Rm, 52.50.Jm

I. INTRODUCTION

Achieving recombination gain is highly desirable in the pursuit of x-ray lasers. Compared to collisional x-ray laser schemes, where a very high degree of ionization is needed, recombination schemes require relatively low pumping power. This, combined with the high quantum efficiency achieved by using the transition to the ground state, makes the creation of a truly tabletop x-ray laser feasible. Furthermore, the highly favorable scaling of the required pumping energy with decreasing wavelengths may enable reaching the so-called “water window” (the wavelength range 2.3–4.4 nm, for which absorption in water is low) with a tabletop x-ray laser system.

However, stringent experimental conditions are required in order to achieve recombination gain. Although several experiments demonstrated gain [1,2] and lasing action [3,4] in the $2 \rightarrow 1$ transition in Li III ions, gain saturation has not yet been achieved. Alongside the experimental efforts, several theoretical studies were conducted in order to identify the processes involved in gain creation, and to characterize the initial conditions required to achieve gain in a recombination scheme (e.g., Refs. [5–8]).

In the case of the Li III $2 \rightarrow 1$ transition, it is fairly straightforward to show from analysis of the rate equations that the required initial conditions for achieving gain are a fully stripped lithium plasma with an electron density in the range 10^{18} – 10^{20} cm $^{-3}$ and an electron temperature under 10 eV. Since the duration of the recombination gain is at most 10–15 psec after ionization, the pumping duration has to be very short in order not to interfere with the recombination process. One of the means of producing such a cold, high density, fully stripped plasma is by optical field ionization (OFI) [5] using an intense, ultrashort laser pulse (pulse duration ~ 100 – 200 fs, intensity $\sim 10^{17}$ W/cm 2). The high electric field in the laser pulse fully strips the Li ions in the plasma, while the short pulse duration prevents substantial heating. Simple estimates can provide the lower limit for the

energy absorbed during the ionization process. For the laser intensities required to reach full ionization, these estimates yield energies that correspond to an electron temperature that is too high for gain to be generated during recombination. Although some of the studies mentioned above include more sophisticated models, which take into account additional effects (such as space charge effects, the effects of different ionizing pulse shapes, and allowing for a two-temperature plasma after ionization), they still predict very small gain (see, e.g., Refs. [7,8]).

We present here results from a numerical model, which takes into account several additional properties of the OFI plasma, such as the non-Maxwellian nature of the plasma and its spatial distribution, and demonstrates that high gain in the $2 \rightarrow 1$ transition of recombining Li III is achievable. Furthermore, we investigate the effects of different experimental parameters on the gain and point toward the optimal experimental conditions required to achieve gain.

II. THEORETICAL BACKGROUND

The main source of heating of OFI plasmas created with ultrashort pulses is the so-called residual heating, or above threshold ionization (ATI) heating [5]. This heating arises from the variation in the oscillation phase ϕ between the ionized electrons [assumed to have zero velocity at the instant of ionization, and then moving with velocity given by $v = v_0 \cos(\omega t + \phi)$] and the phase of the laser electric field. Assuming the ionization occurs by tunneling through the Coulomb barrier in the presence of the electric field, we can calculate the probability of an electron being ionized at a specific laser phase by employing the static electric field tunneling ionization rate (taken from Ref. [9], calculated for the instantaneous electric field). The average residual energy is proportional to the quiver energy of the electrons in the laser field, $\mathcal{E}_q = e^2 E^2 / 4m_e \omega^2$, where e is the electron charge, E is the laser peak electric field, m_e is the electron mass and ω is

the laser angular frequency. We note that the quiver energy is proportional to λ^2 ($\lambda=2\pi c/\omega$). Following Ref. [5], we can extract a functional form of the electron distribution function f_e after ionization:

$$f_e(\eta; E, I_p, \omega) = \frac{a}{\sqrt{\eta(1-\eta)}} \exp\left[\frac{-\frac{2}{3}(I_p/I_h)^{3/2}E_0/E}{\sqrt{1-\eta}}\right], \quad (1)$$

where $\eta=\mathcal{E}/2\mathcal{E}_q$ is the normalized electron energy, I_p is the ionization potential, normalized to the ionization potential of hydrogen atom, I_h , and the electric field E is normalized to the atomic field strength $E_0=5.1\times 10^9$ V/cm. The normalization constant a is determined by the relation $\int_0^1 f_e(\eta; E, I_p, \omega) d\eta = N_e$, where N_e is the electron density. The distribution function in Eq. (1) is derived assuming ionization by a constant-amplitude electric field. The fact that the pulse is actually shaped in time may have a significant effect on the final form of the distribution function and the average energy associated with it. Various pulse shapes and their effects were studied in Ref. [6]. In the model described in Sec. III we assumed the ionizing beam had a Gaussian shape. We note that as $\eta\rightarrow 0$, the distribution function diverges like $\eta^{-1/2}$. Although the divergence disappears as $e-e$ collisions are accounted for, large numbers of electrons are still concentrated in the low-energy region. On the other hand, the distribution has a smooth cutoff at $\eta=1$ and no electrons have energies higher than $2\mathcal{E}_q$. By further examining the behavior as $\eta\rightarrow 1$, we see that for the intensities of interest ($E\sim 2E_0$), the exponential decay of the function for Li III ions corresponds to the exponential decay of a Maxwellian distribution with $\mathcal{E}_{avg}\sim 0.3\mathcal{E}_q$, whereas the average energy of the distribution function in Eq. (1) is only $\mathcal{E}_{avg}\sim 0.15\mathcal{E}_q$. This means that although this part of the distribution function contributes very little to the electron density, it is significantly more populated than it would be for a Maxwellian distribution function, and hence contributes a significant amount to the total average energy. The recombination gain depends upon rapid collisional recombination and deexcitation processes, which are dominated by low-energy electrons. Since most of the electrons are in fact in the low-energy region, the effective recombination rate is higher than would be calculated for a Maxwellian distribution with the same overall average energy.

Figure 1 demonstrates the difference between the calculated distribution function immediately after ionization and a Maxwellian distribution function with the same average energy. The distribution function was calculated using the code described in Sec. III A, for two different ionization wavelengths (248 and 600 nm). The calculation of the function plotted in Fig. 1 has taken into account all the effects discussed below in Sec. III A (including the temporal shape of the ionizing beam and initial conditions of relatively cold He-like Li plasma). Hence, both the shape *and* the average energy associated with the plotted function are very different from the ones associated with the function presented in Eq. (1). We can see that the difference between the calculated and the Maxwellian distribution functions is much more substantial as we increase the wavelength, which is the reason

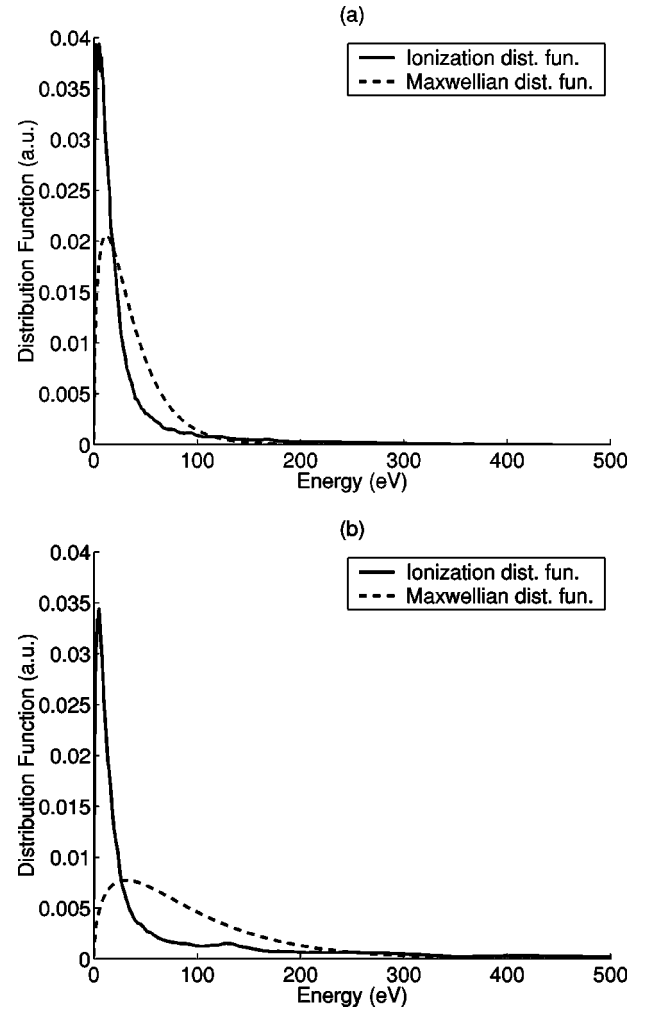


FIG. 1. Electron distribution functions after ionization for different ionizing wavelengths. The solid lines are the calculated distribution functions and dashed lines are Maxwellian distribution functions with the same average energy. In (a) $\lambda=248$ nm and in (b) $\lambda=600$ nm.

that even for longer wavelengths, with average energy of over 100 eV, we can still get large gain. Since the shape of the function is not Maxwellian, the ratio between Maxwellian rates and the rates calculated by direct integration over the distribution function is different for different processes. As an example, we calculated the three-body recombination rates to the different principal quantum levels of Li III, $\beta_{3body}^{(2+)}(n)$, for a distribution function calculated with an ionization wavelength of $\lambda=400$ nm, an ionization intensity of $I_p=1.3\times 10^{17}$ W/cm², and an initial ion density of $N_i=5\times 10^{18}$ cm⁻³. We compared the above rates with the ones calculated for a Maxwellian distribution function with the same average energy (the average energy in this case was $\mathcal{E}_{avg}=64$ eV). The ratio between the rates calculated from the distribution function and the temperature dependent rates was between 3 and 7 for the different principal quantum levels, and averaged to about 5 (averaging on the first ten principal quantum levels). The effects of the non-Maxwellian nature of the OFI plasma were considered before [10], but were not used to calculate gain. One of the main problems

with the above argument was that rapid Maxwellization of the electron distribution may eliminate most of these effects before gain can be generated. However, an additional inherent feature of the plasmas used in the recombination gain experiments is their spatial distribution. In order to achieve the intensities required, the laser beam was focused to a tight spot, roughly $\sim 10 \mu\text{m}$ in diameter, and was then guided through the plasma to create an ionized channel (the “gain region”). This process resulted in a “hot,” high density plasma in a narrow channel embedded in a cold, lower density region. This may have given rise to a rapid expansion and cooling, and resulted in the highly energetic electrons escaping from the gain region without affecting it significantly.

III. NUMERICAL MODEL

The numerical model consists of three distinct stages that are calculated separately. Ionization and heating, expansion and cooling, and recombination and gain (discussed in Secs. III A–III C).

A. Ionization and heating

Ionization is calculated using a 1D (one dimension) in space and 3D in velocity Particle In Cell (PIC) code. The code is parallelized and typically runs on 12 dual CPU nodes. The calculation extends to a radius $r=3r_0$, where r_0 is the ionizing beam radius. In order to simultaneously accommodate the need to have high resolution when calculating the electric field, and the need to have a large number of particles per cell to have good statistics when calculating the collisional processes, the code uses two spatial grids. A coarse grid resolves the beam radius (~ 70 cells per r_0), with an initial 10 000 particles per cell. All particles within each cell interact through binary collisions. A finer grid, which resolves the Debye length, is used to calculate the self-consistent electric field. A minimum initial value of 100 particles per cell is maintained in the finer grid. For different r_0 and different initial plasma densities, the ratio between the cell sizes of the coarse and the fine grids vary, yet the minimum values mentioned above are maintained. At each time step, new particles are added to each cell according to the tunneling ionization rate that corresponds to the instantaneous laser electric field amplitude, presented by

$$\vec{E}_l = E \exp[-(2x/d)^2] \exp[-(2t/\tau)^2] \sin(\omega t) \hat{x}, \quad (2)$$

where \hat{x} is the unit vector of the polarization direction, d is the laser beam diameter, and τ is the pulse duration. Spatial variation is in the \hat{x} direction in order to take into account effects of the ponderomotive force, as discussed below. The initial plasma was taken to be a He-like Li plasma with relatively low (~ 1 eV) electron temperature, which is taken from experimental estimates and agrees with previous calculations [6]. The collision operator models both $e-e$ and $e-i$ collisions, and is implemented using the binary collision model described in Ref. [11]. Special attention was given to the collision frequency under the influence of the strong laser electric field, mainly for establishing the

maximum impact parameter in the Coulomb logarithm. For intense high frequency lasers ($\omega > \omega_p$), the usual Debye shielding, generated in ω_p^{-1} time scales, cannot follow the oscillating electrons and no longer limits the range of the Coulomb potential. The new limiting factor in this case is the requirement that the collision occur in a short time compared with the period of the laser field. The usual parameter used in this case is $b_{max}=v/\omega$ (where v is the electron velocity, see, e.g., Ref. [12]). However, in the cases where the electric field E_l is on the order of the electric field between the ions and the electrons (or higher), another limiting factor for b_{max} needs to be introduced since as the impact parameter increases, the Coulomb field becomes a mere perturbation with respect to the external electric field. We define r_c , the effective maximum Coulomb radius using the relation $e^2/r_c^2 = eZ|\vec{E}_l|$. Our definition for b_{max} is then $b_{max} = \min(\sqrt{eZ/E_l}, v/\omega)$, where the electric field taken is the instantaneous oscillating electric field (in consistency with the requirement that the collision be completed in a short time compared to the laser frequency). In contrast to Refs. [6,10], $e-e$ collisions play an important role in our model. The $e-e$ collision rate is much higher than the $e-i$ collision rate, since the relative velocities between electrons, which are moving together in the electric field, are on the order of the average energy of the final distribution function, whereas the relative velocities between the electrons and the stationary ions are on the order of the electron quiver energy, which is much higher. Although $e-e$ collisions do not contribute to overall heating of the plasma, they do contribute to the Maxwellization process of the distribution function.

Effects of the ponderomotive force are taken into account in the calculation. It was thought that these might significantly affect the gain, especially when the laser was focused very tightly to reduce the diameter of the gain region and increase the expansion and cooling rate. However, the effects of the ponderomotive force turned out to be rather minute, which can be explained by the following analysis. The ponderomotive force is given by

$$f_p = \frac{e^2}{4m_e\omega^2} \vec{\nabla} |E_l|^2. \quad (3)$$

On the other hand, we can estimate the self-consistent electric force f_s in the plasma from Maxwell’s equations. Assuming quasineutrality and taking the beam radius r_0 as the typical length scale in the problem over which we have some density fluctuation δn_e , we can write

$$\vec{\nabla} \cdot \vec{E} = 4\pi\rho \Rightarrow f_s \sim 4\pi e^2 r_0 \delta n_e. \quad (4)$$

Considering the ratio of the two forces (the ponderomotive force f_p is taken at its maximum point, $r=r_0/\sqrt{2}$) we have

$$\frac{f_s}{f_p} \sim 7.5 \tilde{n}_e \left(\frac{r_0}{\lambda} \right)^2 \frac{\delta n_e}{n_e}, \quad (5)$$

where \tilde{n}_e is given in units of 10^{19} cm^{-3} . With $\tilde{n}_e=1$ and a typical value for r_0/λ of about 5 (for a tightly focused

beam), we see that the ponderomotive force can induce density fluctuations of no more than 1%, and is therefore negligible.

B. Expansion and cooling

As shown in Ref. [10], the distribution function produced by OFI yields very high recombination rates, which may lead to very high gain. However, since the Maxwellization process is very rapid, the net effect on the gain may be substantially smaller. As discussed above, the fully ionized plasma is only created within a narrow channel, about $10\ \mu\text{m}$ in diameter, which is embedded in a low temperature, lower density plasma. Hence, the hot fully ionized plasma undergoes rapid expansion and cooling that affects the distribution function on time scales relevant for gain generation, i.e., 10-15 psec after ionization. Furthermore, this expansion significantly slows down the Maxwellization process, since the electrons — especially the energetic electrons — tend to escape the gain region before colliding with any of the particles there. The time evolution of the distribution function following ionization is calculated using a 1D cylindrically symmetric Fokker-Planck code. The code, described in Ref. [13], is essentially an implementation of the SPARK code [14]. The assumption of cylindrical symmetry is somewhat inaccurate, but conservative, since relaxing this assumption is expected to lead to faster cooling and higher gain. This is because the velocities of the electrons that were ionized by a linearly polarized laser beam are directed straight out of the gain region and not isotropically distributed as in our model, therefore the energetic electrons have a higher probability than we calculate to escape the gain region without affecting it. In order to stay within the diffusion approximation, we introduced a smooth cutoff to the distribution function at high energies. The cutoff was introduced for energies above 500 eV, for which $v\tau_c/r_0 \gg 1$ (where v is the velocity associated with 500 eV and τ_c is the collision time), since particles with such high energies have very little probability of participating in any collisional process inside or close to the gain region. Finally, although recombination physically occurs simultaneously with expansion, it is calculated within a separate code with no feedback. Hence, effects from recombination heating were not taken into account in the calculation of the expansion and cooling of the plasma. However, an estimate (see below) of the overall heating from recombination clearly shows that it should have no significant effect on the expansion and cooling processes or the gain.

C. Recombination and gain

In order to take into account the effects of the non-Maxwellian nature of the distribution function, the cross sections for the relevant atomic processes are integrated over the time-dependent distribution function, yielding time-dependent rate coefficients, which are used to calculate the recombination processes and gain. In order to simplify the code and make it more robust, simple analytic forms for the ionization and excitation cross sections were used [15,16]. The other required cross sections were obtained from the

detailed balance relations between excitation (ionization) and deexcitation (recombination) processes.

In order to estimate plasma heating due to recombination and deexcitation processes, we examined at the time-dependent level populations, and calculated the energy addition from all the recombined electrons (up to the time when the maximum gain is achieved) according to the relation

$$\langle \varepsilon \rangle(t) = \frac{1}{N_e(t)} \sum_n N_n^{(+2)}(t) I_{p,n}, \quad (6)$$

where $N_n^{(+2)}(t)$ is the population of level n of the Li III ions at time t , and $I_{p,n}$ is the ionization potential from level n . The estimated heating did not exceed 0.5 eV for any of the parameters considered, and was under 0.1 eV in most of the cases. We should note that in dividing by N_e we assumed that the added energy is distributed equally among all the electrons. In fact, since the electrons contributing to the recombination are, in essence, the low-energy electrons, they are the ones that will absorb the added energy. However, as discussed above and shown in Fig. 1, the low-energy electrons are the majority of the electrons and even if the heating were twofold or threefold higher than given by Eq. (6), it would not be expected to affect the gain significantly.

IV. RESULTS FROM THE NUMERICAL MODEL

The model described above is used to compute a 1D space-time distribution of the recombination gain in the Li III $2 \rightarrow 1$ transition. We investigated the gain as a function of the four main parameters that influence it in the following parameter range: Plasma ion density, $10^{18} - 5 \times 10^{19}\ \text{cm}^{-3}$ (Sec. IV A); ionizing beam diameter, $6 - 15\ \mu\text{m}$ (Sec. IV B); ionizing beam wavelength, 248, 400, and 600 nm (Sec. IV C); and ionizing beam intensity, $1.3 - 2.2 \times 10^{17}\ \text{W/cm}^2$ (Sec. IV D).

A. Plasma density

Since both the gain and the rates of the underlying atomic processes increase with higher electron density, we expect higher gain of shorter duration at higher densities. Indeed, as can be seen in Fig. 2, the gain increases significantly as the density increases, and the duration of the gain is shortened. At the highest density [Fig. 2(d)], we note that high gain is seen immediately after the ionization. Since the effects of recombination during ionization, which are more probable in the high density case, are not taken into account in the model, the actual results presented in this part of the figure should be treated with caution. It is presented for qualitative purposes only.

B. Ionizing beam diameter

The beam diameter determines the cooling rate, and more importantly, the effective delay in the Maxwellization rate, due to the escape of the energetic electrons from the gain region before participating in any Maxwellization process. Therefore we can expect the gain to grow as the beam radius is decreased. However, it is harder to propagate a tightly

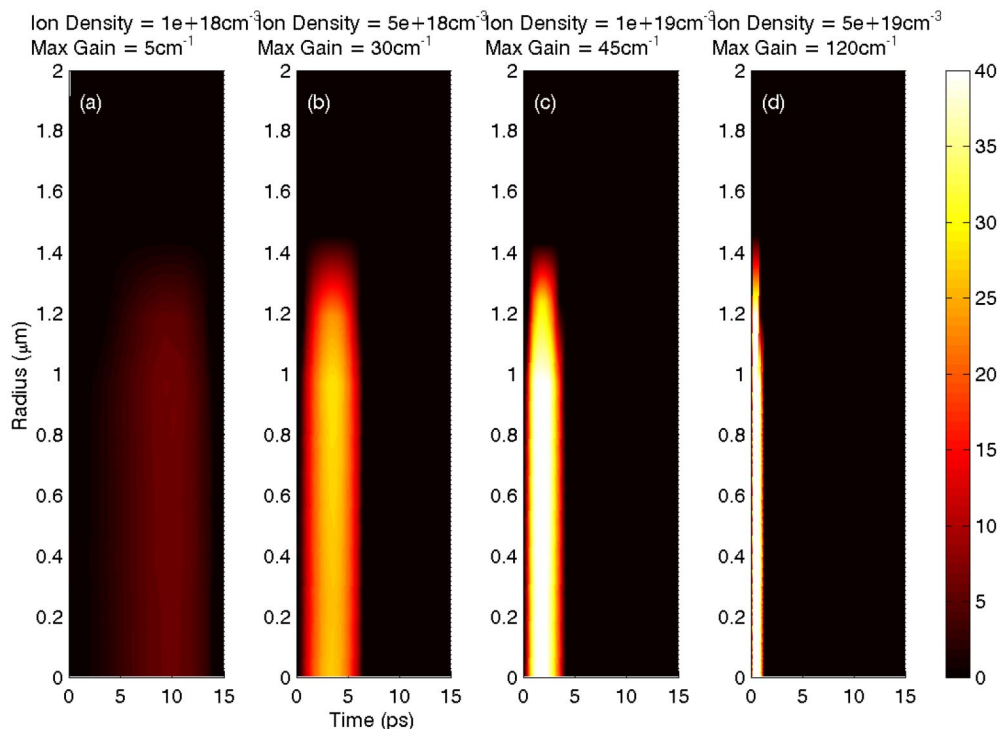


FIG. 2. (Color online) Gain distribution for different ion densities N_i . The ionizing beam wavelength in all cases is $\lambda=248$ nm, the beam diameter is $d=10 \mu\text{m}$, and the beam intensity is $I_p=1.3 \times 10^{17}$ W/cm². N_i (in units of 10^{18} cm⁻³): (a) 1, (b) 5, (c) 10, and (d) 50.

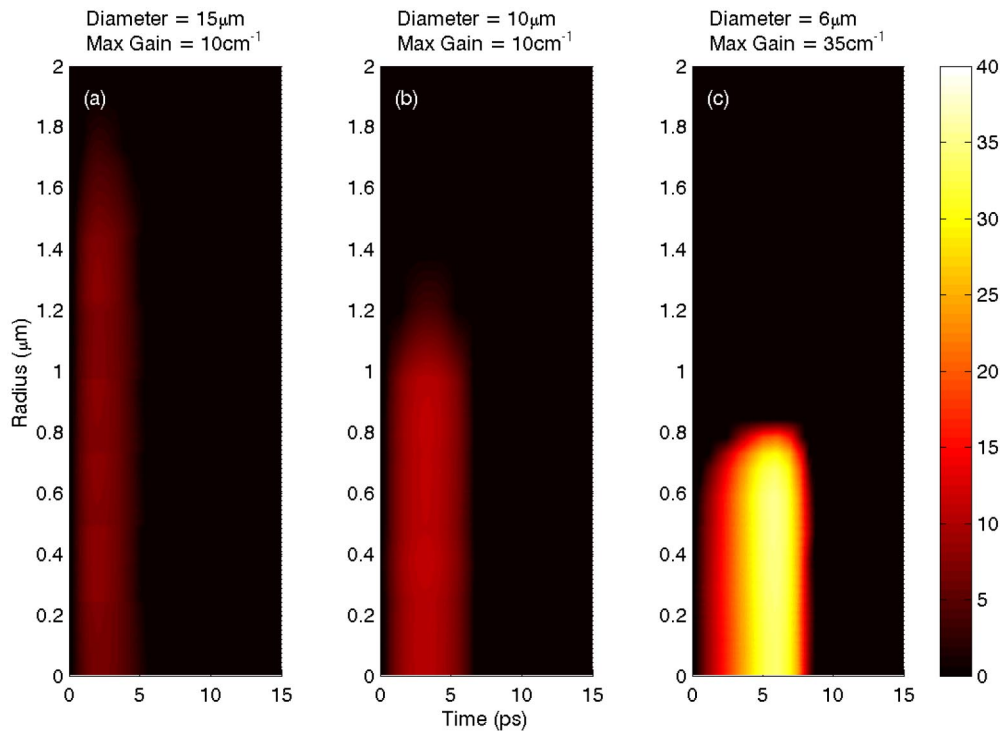


FIG. 3. (Color online) Gain distribution for different ionization beam diameters d . The ion density in all cases is $N_i=5 \times 10^{18}$ cm⁻³, the beam wavelength is $\lambda=400$ nm, and the intensity is $I_p=1.3 \times 10^{17}$ W/cm². (a) $d=15 \mu\text{m}$, (b) $d=10 \mu\text{m}$, (c) $d=6 \mu\text{m}$.

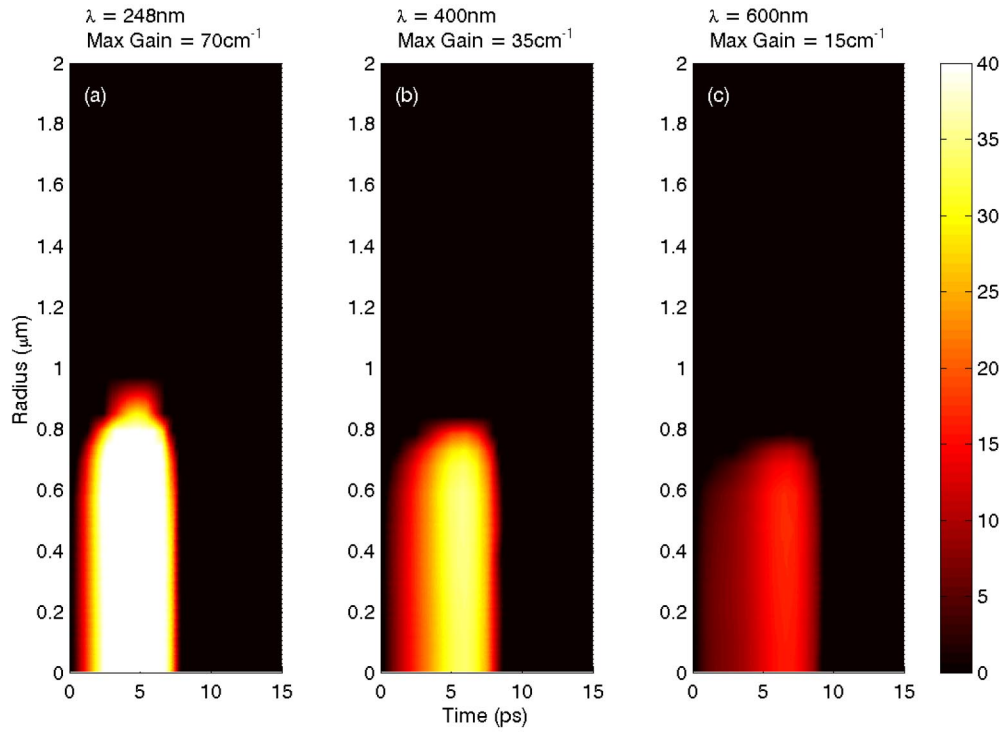


FIG. 4. (Color online) Gain distribution for different ionization beam wavelengths λ . The beam diameter in all cases is $d=6 \mu\text{m}$, the intensity is $I_p=1.3 \times 10^{17} \text{ W/cm}^2$, and the ion density is $N_i=5 \times 10^{18} \text{ cm}^{-3}$. (a) $\lambda=600 \text{ nm}$, (b) $\lambda=400 \text{ nm}$, (c) $\lambda=248 \text{ nm}$.

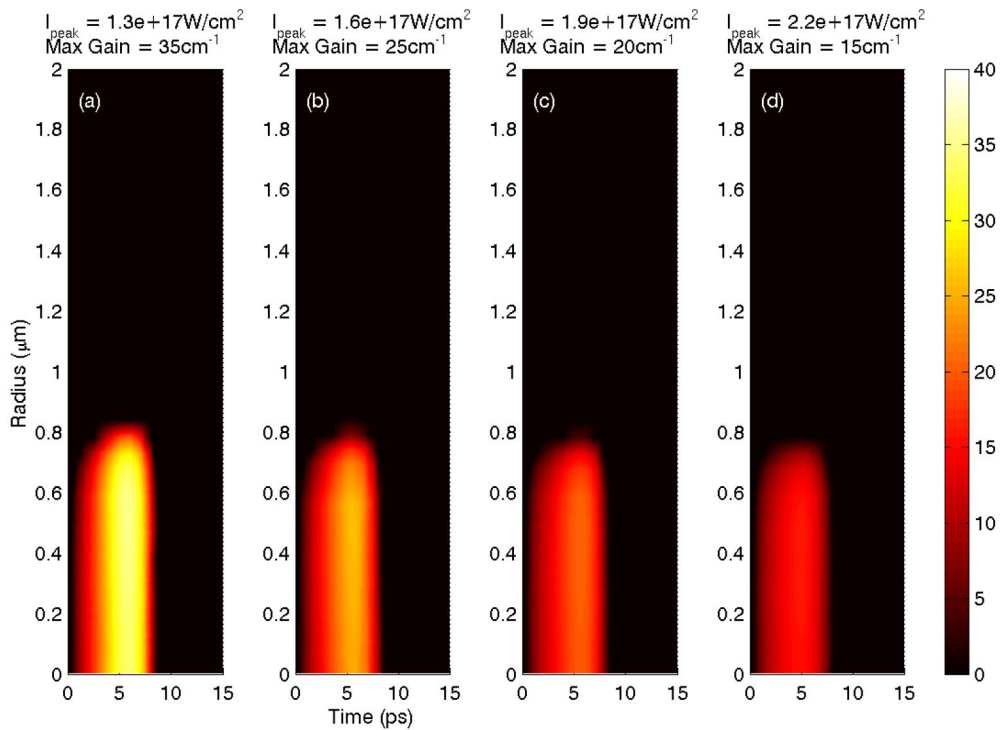


FIG. 5. (Color online) Gain distribution for different ionizing beam peak intensities I_p . The beam wavelength for all the runs was $\lambda=400 \text{ nm}$, the beam diameter was $d=6 \mu\text{m}$, and the ion density was $N_i=5 \times 10^{18} \text{ cm}^{-3}$. I_p (in units of 10^{17} W/cm^2): (a) 1.3, (b) 1.6, (c) 1.9, and (d) 2.2.

focused beam, which is one of the crucial experimental difficulties in producing recombination gain. The results of the gain for different beam diameters are presented in Fig. 3.

C. Ionizing beam wavelength

As discussed in Sec. II, the energy absorption by the plasma during ionization is due to the so-called residual, or ATI, heating. The average energy is proportional to λ^2 , so using a longer wavelength ionizing beam should cause further heating and decrease the gain substantially. In Fig. 4 we see, however, that although the gain indeed drops substantially when we increase the wavelength, the gain persists even up to a wavelength of 600 nm.

D. Ionizing beam intensity

The gain is very sensitive to the initial conditions of a fully ionized plasma. The fractional occupation of the $n=2$ level does not exceed about 10^{-3} in times relevant for gain generation, and by taking into account the statistical weight factor, we find that a fraction of $\sim 10^{-4}$ of not fully ionized ions will destroy the gain. Hence, there exist an intensity threshold, or a minimum intensity, for which we can achieve gain. On the other hand, the average energy of the OFI

plasma is proportional to the beam intensity, and we expect lower gain for higher intensity pump beams. The optimal ionizing intensity is then just above the “cutoff intensity.” In a longitudinal pumping setup, the ionizing beam is absorbed during the propagation and ionization, hence the intensity has to be adjusted so that at the exit of the channel, it will still be above the cutoff intensity. The gain for different intensities shown in Fig. 5 is a way of demonstrating the behavior of the gain along the channel, considering longitudinal pumping. We can think of the pumping beam as traveling from right to left in Fig. 5, being absorbed as it propagates. Each plot shows the gain cross section at a different point along the propagation, with the smallest gain at the entrance and the highest gain at the exit of the plasma.

ACKNOWLEDGMENTS

We are very thankful to G. Pert (York University, UK) for very stimulating discussions and for providing us with some of his papers that are not yet published. The comments about the ponderomotive force from E. Fill (Max Planck Inst., Germany) were highly appreciated. This work was supported by INTEL and NSF (physics) and by a financial support from PU/PPPL Plasma Science and Technology.

-
- [1] Y. Nagata, K. Midorikawa, S. Kubodera, M. Obara, H. Tashiro, and K. Toyoda, *Phys. Rev. Lett.* **71**, 3774 (1993).
 - [2] K. M. Krushelnick, W. Tighe, and S. Suckewer, *J. Opt. Soc. Am. B* **13**, 306 (1996).
 - [3] D. V. Korobkin, C. H. Nam, S. Suckewer, and A. Goltsov, *Phys. Rev. Lett.* **77**, 5206 (1996).
 - [4] A. Goltsov *et al.*, *IEEE J. Sel. Top. Quantum Electron.* **5**, 1453 (1999).
 - [5] N. H. Burnett and P. B. Corkum, *J. Opt. Soc. Am. B* **6**, 1195 (1989).
 - [6] K. A. Janulewicz, M. J. Grout, and G. J. Pert, *J. Phys. B* **29**, 901 (1996).
 - [7] K. A. Janulewicz, S. B. Healy, and G. J. Pert, *Opt. Commun.* **140**, 165 (1997).
 - [8] G. J. Pert, *J. Phys. IV* **11**, 181 (2001).
 - [9] A. M. Perelomov, V. S. Popov, and M. V. Terent'ev, *Sov. Phys. JETP* **23**, 924 (1966).
 - [10] T. Ditmire, *Phys. Rev. E* **54**, 6735 (1996).
 - [11] T. Takizuka and H. Abe, *J. Comput. Phys.* **25**, 205 (1977).
 - [12] G. J. Pert, *Phys. Rev. E* **51**, 4778 (1995).
 - [13] S. Brunner and E. Valeo, *Phys. Plasmas* **9**, 923 (2002).
 - [14] E. M. Epperlein, *Laser Part. Beams* **12**, 257 (1994).
 - [15] W. Lotz, *Z. Phys.* **216**, 241 (1968).
 - [16] V. I. Fisher, Y. V. Ralchenko, V. A. Bernshtam, A. Goldgirsh, Y. Maron, L. A. Vainshtein, I. Bray, and H. Golten, *Phys. Rev. A* **55**, 329 (1997).